

Journal of Materials Chemistry A

Accepted Manuscript



This is an *Accepted Manuscript*, which has been through the Royal Society of Chemistry peer review process and has been accepted for publication.

Accepted Manuscripts are published online shortly after acceptance, before technical editing, formatting and proof reading. Using this free service, authors can make their results available to the community, in citable form, before we publish the edited article. We will replace this *Accepted Manuscript* with the edited and formatted *Advance Article* as soon as it is available.

You can find more information about *Accepted Manuscripts* in the [Information for Authors](#).

Please note that technical editing may introduce minor changes to the text and/or graphics, which may alter content. The journal's standard [Terms & Conditions](#) and the [Ethical guidelines](#) still apply. In no event shall the Royal Society of Chemistry be held responsible for any errors or omissions in this *Accepted Manuscript* or any consequences arising from the use of any information it contains.

Toward “Rocking-chair type” Mg-Li Dual-salt Battery

Tetsu Ichitsubo,^{1*} Shinya Okamoto,¹ Tomoya Kawaguchi,¹ Yu Kumagai,² Fumiyasu Oba,^{1,2} Shunsuke Yagi,³ Natsumi Goto,¹ Takayuki Doi,⁴ Eiichiro Matsubara¹

¹Department of Materials Science and Engineering, Kyoto University, Kyoto 606-8501, Japan

²Materials Research Center for Element Strategy, Tokyo Institute of Technology, Yokohama 226-8503, Japan

³Nanoscience and Nanotechnology Research Center, Osaka Prefecture University, Osaka 599-8570, Japan

⁴Department of Molecular Chemistry and Biochemistry, Doshisha University, Kyoto 610-0321, Japan

High energy-density rechargeable batteries are strongly demanded from the viewpoint of energy and environmental concern. This work is devoted to fundamental electrochemistry on a novel concept of rechargeable battery, “rocking-chair type” Mg-Li dual-salt battery (DSB), where both Mg and Li cations are carrier ions. In this system, dangerous dendritic growth is drastically suppressed by co-electrodeposition of Mg and Li, and Mg-Li alloys can be used as anode materials with high electrical capacities. As a DSB cathode material that can accommodate both Mg and Li cations, we use a spinel oxide MgCo_2O_4 , in which an eccentric insertion mechanism, “intercalation & push-out” process, occurs. Mg insertion occurs at 2.9 V vs. Mg^{2+}/Mg and Li insertion does at 3.1 V vs. Li^+/Li , being consistent with *ab initio* calculations, and its capacity approximately amounts to 150–200 mAh g^{-1} . In the combination of MgCo_2O_4 and $\text{Mg}_{50}\text{Li}_{50}$ alloy, the cell voltage during discharge is as high as about 2–3 V. The concept of rocking-chair type DSB systems provides a new strategy for future safe rechargeable batteries combining high energy/power densities.

Polyvalent less-noble metals, e.g., Mg, Ca, and Al, have attracted much attention as an anode material for polyvalent-metal rechargeable batteries, because their theoretical capacities (e.g., 2200 mAh g^{-1} for Mg) are much higher than those (about 370 mAh g^{-1}) of carbonaceous materials currently used in LIBs. Especially, since it was found that the Chevrel compound, $\text{Mg}_2\text{Mo}_6\text{S}_8$, could be used as a cathode material of magnesium rechargeable batteries (MRBs),¹ MRBs have attracted growing attention not only due to the low redox potential of Mg, but also due to its abundance, inexpensiveness, and relatively safe handling. Above all, the most advantageous point of MRBs is that Mg metal can be adopted as an anode material, because the non-dendritic (i.e., smooth or plate-like) electrodeposition can be attained upon charge unlike Li anode, which can avoid a fatal concern about short circuit.^{2–5}

Recently, Ichitsubo and Yagi et al.⁶ reported a concept of Daniell-type dual-salt battery (DSB) that contains Mg and Li dual salts in a tetrahydrofuran electrolyte, then followed by some independent researchers.^{7–9} In the Daniell-type DSB systems, the redox reaction associated with Li occurs at the cathode and that associated with Mg takes place at the anode. Although such Daniell-type battery cannot enhance the energy density due to requirement of huge amount of electrolyte, they have clearly shown a significant advantage of DSBs in that the fatal problem of dendritic electrodeposition is drastically suppressed even at a sufficiently low potential at which Li metal can be electrodeposited on charge. This superior feature on the anode morphology can be obtained for various electrolyte systems; see Fig. 3S in Supplementary Information (SI).

In this work, we propose a “rocking-chair type” DSB concept, where Mg and Li cations can be both carriers in the battery so that the two kinds of cations in a Mg-Li alloy anode can be transferred to a cathode active material, and vice versa, which can reduce dramatically the amount of electrolyte unlike the Daniell-type DSB system; Fig. 1 clearly illustrates this concept. Here, we basically used CsTFSA-based mixed ionic liquids as an electrolyte that can endure at about 200–300 °C,¹⁰ to conduct electrochemical tests at about 150 °C for the spinel oxide cathode materials recently reported by the present authors.¹¹ As shown in optical and SEM micrographs in Fig. 1, a critical issue of dendritic morphology was also confirmed on charge at 150 °C in using a binary (Li10/Cs90)-TFSA ionic liquid (the molar ratio of LiTFSA/CsTFSA is 10/90), where CsTFSA plays a role of a solvent. As opposed to this, in us-

ing a ternary (Li10/Mg10/Cs80)-TFSA ionic liquid, we can obtain a very smooth non-dendritic morphology in the co-electrodeposited Li-Mg alloy, despite setting at a sufficiently low potential (–0.5 V vs. Li^+/Li in RE: RE means the Li reference electrode in a separated glass tube), at which Li metal can be electrodeposited; the atomic ratio of the electrodeposited alloy was measured to be $\text{Li}/\text{Mg}/\text{Cs} = 1.9/1/(0.2)$ by the inductively coupled plasma (ICP)

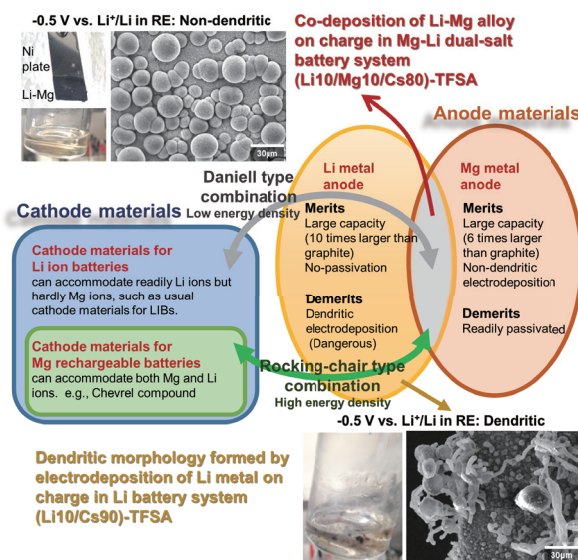


FIG. 1: Concept of Mg-Li dual-salt battery system based on the anode characteristics. The respective merits and demerits of Li and Mg batteries are illustrated with scanning electron and optical microscope images of the electrodeposited Li metal in (Li10/Cs90)-TFSA (lower) and Li-Mg alloy (Li10/Mg10/Cs80)-TFSA (upper). In the case of electrodeposition of Li metal, dendritic morphology is observed and fragments of Li metal remain in the beaker cell. In contrast, in the Mg-Li dual-salt system, the dendrite formation was significantly suppressed on charge. The Daniell-type combination of cathode materials for Li batteries with Mg-Li alloy anode cannot enhance the energy density, but the rocking-chair type combination of cathode materials for Mg batteries with Mg-Li alloys would enhance the energy density effectively.

*Corresponding: tichi@mtl.kyoto-u.ac.jp

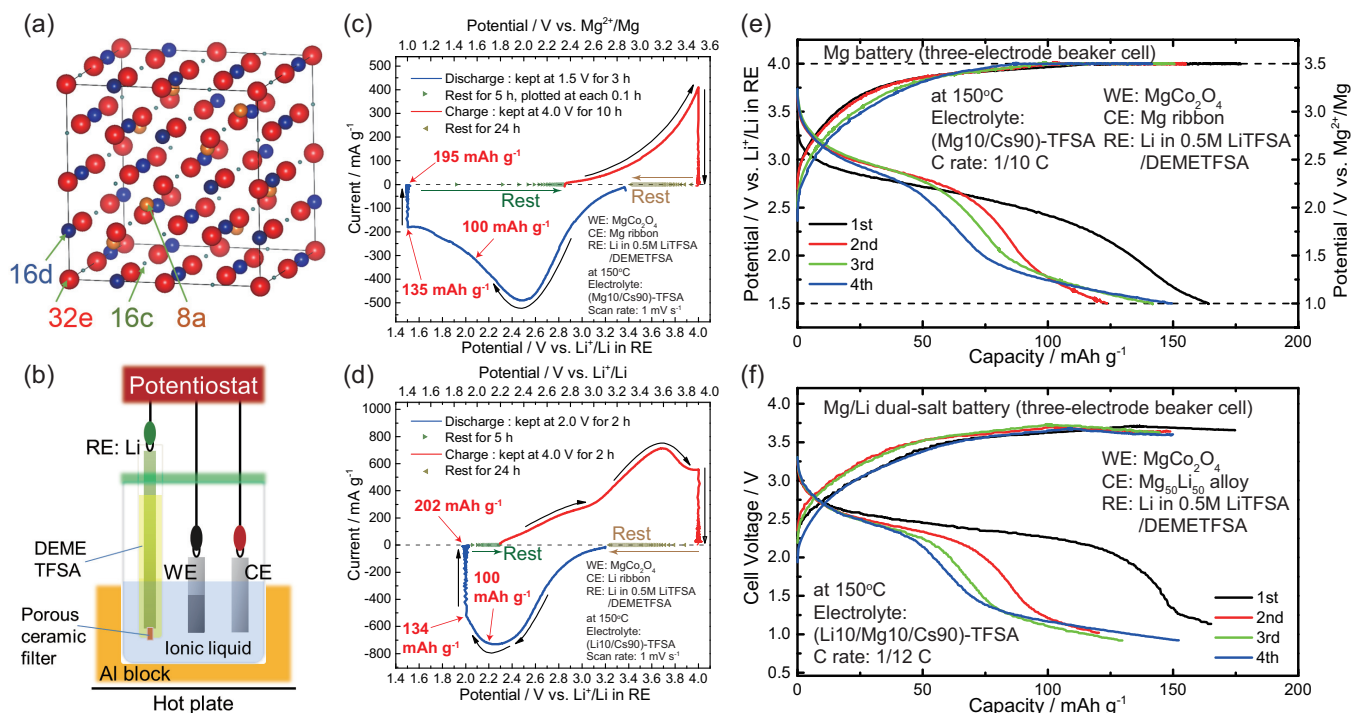


FIG. 2: (a) Spinel structure depicted by setting a 32e site at origin. (b) Typical three-electrode beaker cell used here, where Li metal immersed in a 0.5 M-LiTFSA/DEMETFSA electrolyte in a glass tube separated with a porous ceramic filter was used as the reference electrode (RE). Cyclic voltammograms with chronoamperometry (CVA) at 150°C of MgCo_2O_4 for (c) Mg insertion/extraction and (d) Li insertion/extraction processes. The ionic liquids of $\text{Mg}(\text{TFSA})_2/\text{CsTFSA} = 1/9$ and $\text{LiTFSA}/\text{CsTFSA} = 1/9$ (mol ratio) were used for the Mg and the Li batteries, respectively. The potential conversion rule is described in SI. Battery cycle tests (e) for the Mg battery system, WE: MgCo_2O_4 , CE: Mg, RE: Li in a separate glass tube, and (f) for the Mg/Li dual-salt battery system, WE: MgCo_2O_4 , CE: Mg-Li alloy, RE: Li in a separate glass tube. Cut-off conditions in the battery tests were made based on the WE potential. In the cathode active material after the battery test, the insertion-amount ratio of Mg and Li was measured to be $\text{Mg}/\text{Li} = 7/5$ by ICP.

analysis. In addition, there is no metal segments fallen off from the electrode in the beaker cell. Thus, it is clearly shown that this anode morphology of co-electrodeposition of Mg-Li alloy is quite superior to the Li dendritic morphology.

Apparently, as illustrated in Fig. 1, rocking-chair type DSB systems inevitably require cathode materials that can accommodate not only Li but also Mg cations. Since MRB cathode materials like Chevrel compounds that can accommodate divalent Mg ions would do monovalent Li ions as well,^{7,12,13} consequently we need to seek cathode materials for MRBs. Despite that several candidates for the cathode materials of MRBs have been reported,^{14–16} currently only Chevrel compounds^{1,12} can show superior intercalation/deintercalation characteristics at ambient temperatures. Thus, currently there are few cathode materials for MRBs, and even if the Chevrel compounds are used, the theoretical electrode energy density of the MRB system is less than 150 mWh g^{-1} (much less than about 370 mWh g^{-1} in a combination of LiCoO_2 vs graphite). In this study, as a cathode material for DSB, we use a spinel oxide MgCo_2O_4 with a higher theoretical capacity 260 mAh g^{-1} (actually about 200 mAh g^{-1} at 1/20 C) and redox potential approximately 3 V vs. Mg^{2+}/Mg , where the eccentric insertion mechanism, termed “intercalation & push-out” process, takes place.¹¹

To see fundamentally the electrochemical phenomena in electrochemicals, we have to construct three-electrode beaker cells; a typical construction of beaker cells used here is illustrated in Fig. 2(b), where Li-metal ribbon immersed in a glass tube separated by a ceramic filter was used as a reference electrode (RE). Figures 2(c) and 2(d) show the cyclic voltammetry with chronoamperometry (CVA) profiles for Mg and Li insertion/extraction processes, respectively;

the constant potentials in the chronoamperometry were set at 1.5 V and 2.0 V vs. Li^+/Li in RE for Mg and Li insertions, respectively, by taking into account the difference in the current densities. Usually one would consider the conventional reaction of Mg extraction from the host material. However, in this work, without a pre-charge process we directly inserted Mg cations into a host MgCo_2O_4 active material, by utilizing 16c-site vacancies in the spinel structure¹¹. It is clearly seen that Mg and Li insertions can occur into the host MgCo_2O_4 and then these cations can be reversibly extracted during a charge process; see Fig. S2 in SI for cyclic voltammograms (incidentally, as seen in Table S1 in SI, Cs cations can hardly be inserted into MgCo_2O_4). The equilibrium redox potentials for the insertion/extraction of Mg and Li cations are estimated to be about 2.9 V vs. Mg^{2+}/Mg (3.4 V vs. Li^+/Li in RE) and 3.1 V vs. Li^+/Li (3.2 V vs. Li^+/Li in RE), respectively; see Fig. S1 in SI for the potential conversion rules. Despite the current difference, the insertion amounts obtained by sweep down to about 2.0–2.2 V are about 100 mAh g^{-1} in both the cases. Eventually, through the constant-potential discharge process, the capacities reached about 200 mAh g^{-1} in both the cases (theoretically 260 mAh g^{-1}). The similar electrochemical reactions were observed in other spinel oxide compounds, MgMn_2O_4 , Co_3O_4 , etc.¹¹ In contrast to the Mg insertion/extraction, two distinct stages are clearly observed in the extraction process of Li. This is due to the difference between the monovalent Li cation and divalent Mg cation; two Li cations can be inserted into the spinel structure due to the reduction from Co(III) to Co(II) of two Co cations in MgCo_2O_4 , but the Li cation already inserted at a 16c site needs to move slightly to accommodate an extra Li cation, which is described later. During the rest time, the

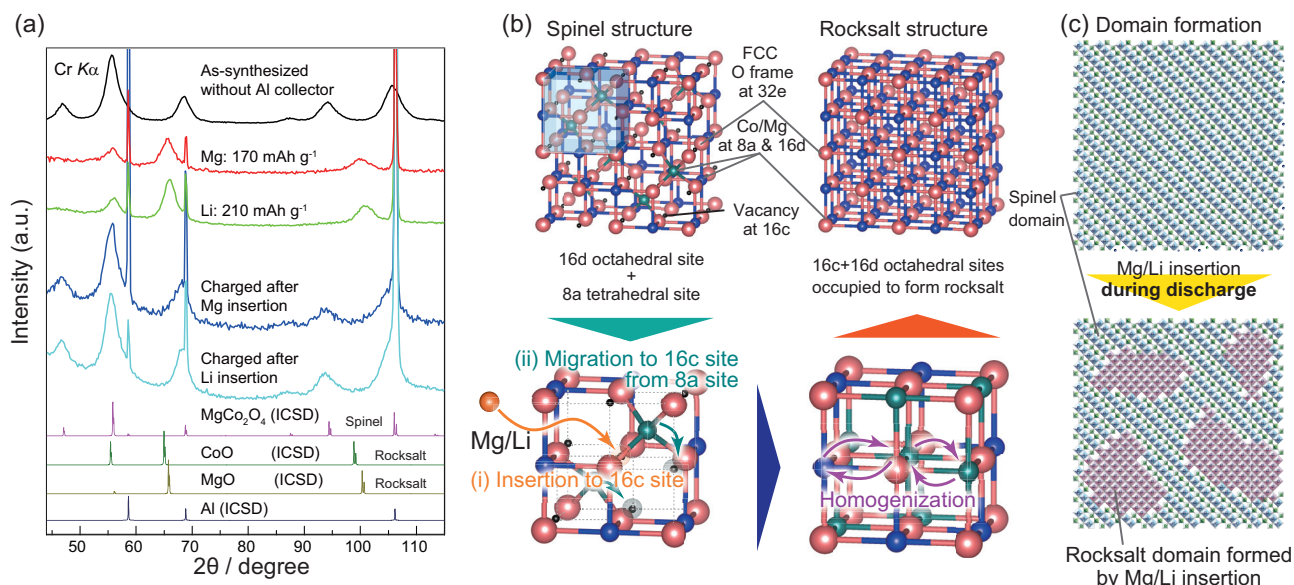


FIG. 3: (a) XRD profiles obtained after deep discharge (about 170–210 mAh g^{-1} by Mg and Li insertions) and successive charge after insertion to the same extent. After the insertions of Mg and Li, the active materials substantially show rocksalt structures in both the cases, and then after charge the rocksalt phase undergoes the reversible transformation to the original spinel phase. (b) Schematic illustration showing the cation insertion and transformation process. In the spinel structure, where a 32e site is set at origin, 8a, 16c, 16d, and 32e show the Wyckoff positions in $Fd\bar{3}m$ (space group No. 227), and usually 16c sites (marked by small black circles) are vacant in spinel structures. After a Mg or Li cation is inserted into a 16c site in the spinel structure, the original cation located in its neighboring 8a site moves to an adjacent 16c site due to the electrostatic repulsion between the cations, to form a rocksalt structure. This fundamental process occurs within the framework of the spinel structure, and the phase change occurs coherently. (c) After continuous insertion of cations, atomic-level rocksalt domains are formed in the spinel structure, resulting in the coherent phase separation.

open circuit potential (OCP) recovered rapidly to the initial OCP value in the Mg case, while it does not revert in the rest time in the case of Li.

Figure 2(e) shows the constant-current battery performance test for a Mg battery; the electrode potential of WE was monitored versus RE. Also in this case, the battery test is able to start from the discharge process. Although the cathode material is seemingly degraded with the cycle number, this is mainly due to the following two reasons: the low thermal stability of the PVDF binder and the oxidation decomposition of the electrolyte during charge (the oxidation limit of electrochemical window is about 4 V vs. Li^+/Li in RE). Thus, to settle the problem of the capacity fading is a future work. In the 1st discharge process, the converted working potential is shown to be 2–2.5 V vs. Mg^{2+}/Mg , and the capacity amounts to about 120 mAh g^{-1} above 2 V vs. Mg^{2+}/Mg and also amounts to 170 mAh g^{-1} above 1 V vs. Mg^{2+}/Mg at a rate of 1/10 C. In this battery system, however, the Mg anode is readily passivated in the (Mg10/Cs90)-TFSA ionic liquid, so that its anodic dissolution comes to occur above 1.5 V vs. Li^+/Li in RE, which leads to an unfortunate consequence that the cell voltage decreases with the passivation of the Mg anode.¹⁷

However, we can completely exploit the high potential of the cathode material in the Mg-Li dual-salt battery. Figure 2(f) shows the cell voltage versus capacity curve obtained for a Mg-Li dual-salt battery. In the Mg-Li dual-salt battery, an $\text{Mg}_{49}\text{Li}_{51}$ alloy in atomic ratio was used for the anode material, and the ternary ionic liquid of (Li10/Mg10/Cs80)-TFSA (atomic ratio of cations) was used for the electrolyte. In this case, surprisingly the anodic dissolution of the Mg-Li alloy can occur at reasonably low potentials about 0.5–0.6 V vs. Li^+/Li in RE (note that the anodic dissolution potential is much lower than the potential (~ 1.5 V vs. Li^+/Li in RE) of the passivated Mg electrode; the anodic dissolution behavior of the BCC Mg-Li alloy is shown in Fig. S5 in SI. Thus, it is shown that alloying of Mg with Li would be effective to cir-

cumvent the electrode passivation, and consequently we can obtain an excellent cell voltage of about 2–3 V during a discharge process. Nevertheless, in the near future, we have to figure out the passivation problem of the Mg-metal electrode by creating a more excellent electrolyte for MRBs that essentially cause no passivation. The atomic composition of the MgCo_2O_4 cathode after the final discharge in the battery test indicates that almost the same quantity of Mg and Li cations (atomic ratio in the cation insertion: $\text{Mg}^{2+}/\text{Li}^+ = (1.6-0.9)/(0.5-0) \sim 7/5$) were inserted into the active materials and Cs cations can hardly be inserted; See Table S1 in SI. This means that the capacity by the divalent Mg cations is more than twice of that by the monovalent Li cations, and thus the roles of Mg cations are significant not only for the anode morphology but also for the high potential of the cathode reaction.

To understand the cation-insertion mechanism, we conducted structural analyses before/after battery tests. As shown in Fig. 3(a), after a sufficiently large amount of discharge (about 170–210 mAh g^{-1}), mostly a rocksalt phase can be detected in the XRD profiles for both Mg-insertion and Li-insertion processes. The fact that the spinel phase disappears even at such an incomplete discharge amount less than the theoretical value (260 mAh g^{-1}) means that the rocksalt phase includes a certain amount of cation vacancies; a solid-solution phase of off-stoichiometry exists. It is naturally expected that MgCoO_2 of a random solution type rocksalt phase is formed in a final state after the Mg insertion, since both of MgO and CoO have similar rocksalt structures. However, interestingly, also in the Li insertion process, the structure of MgCo_2O_4 changes from spinel to rocksalt. In both cases, by successive charge, the discharged rocksalt phase reverts to the initial spinel phase, which suggests that Co(II) cations with a larger ionic radius than that of Mg cations are hardly extracted from the host material during the charge process, because, if not so, the spinel structure cannot be retrieved; the Mg cations remaining in the spinel structure cannot compensate the electrical charge (within the $\text{II} \leftrightarrow \text{III}$

valence change of Co). As to the Mg insertion and extraction, we have confirmed the valence change of the transition metals by the XANES measurement.¹¹

To complement the experimental findings, *ab initio* calculations were performed using the GGA+*U* approach; see Methods and SI for details. At the beginning, we searched for the most stable spin and magnetic configurations in various atomic configurations of spinel MgCo_2O_4 , and then, Mg or Li were inserted to create $\text{Mg}_2\text{Co}_2\text{O}_4$ and $\text{MgLiCo}_2\text{O}_4$ models. Since MgCo_2O_4 is a disordered spinel, we considered all possible cation configurations in the primitive unit cell. We started geometry optimizations from two sets of initial structures; after placing of Mg or Li atoms at 16c sites, we artificially displaced their neighboring cations being located at 8a sites to 16c sites to form rocksalt structures for the first set, and left them intact for the second set. The most stable magnetic configurations were also determined in the rocksalt structures, and the redox potentials were estimated for all the configurations. Eventually, most of tested atomic configurations of $\text{Mg}_2\text{Co}_2\text{O}_4$ and $\text{MgLiCo}_2\text{O}_4$ converged to the rocksalt structures, whose averaged lattice constants estimated from the cell volume changed by the cation insertion to 8.54 Å and 8.43 Å (twice the lattice constant of the rocksalt) from 8.38 Å of spinel MgCo_2O_4 , respectively, which are in qualitative agreement with the XRD data.

The average redox potentials for Mg and Li insertion are calculated to be 3.0 V vs. Mg^{2+}/Mg and 3.4 V vs. Li^+/Li , respectively. The former excellently agrees with the experimental potential of 2.9 V vs. Mg^{2+}/Mg , but the latter shows slight discrepancy from the experimental value. The lower experimental value of 3.1 V vs. Li^+/Li compared to the theoretical redox potential would be attributed to excess Li insertion in the experiment. In view of the insertion capacity of monovalent Li cations, further Li ions can be inserted into rocksalt $\text{MgLiCo}_2\text{O}_4$. Actually, the CVA profile for Li insertion/extraction processes in Fig. 2(d) shows a double peak feature compared to that for Mg insertion/extraction processes. Thus, Li insertion/extraction process is, in principle, composed of two stages. To comprehend these observations, we further modeled $\text{Li}_{1.5}\text{MgCo}_2\text{O}_4$ containing excess Li ions and calculated its redox potential. In the initial structures, the excess Li ions were set at 8a sites (Wyckoff positions based on the original spinel structure). Through the geometry optimization, as seen in Fig. S6, in some structures, the original Li cations at 16c moved to off-sites to form dimers with the Li cations originally located at the adjacent 8a, and in other structures, the original Li at 16c and extra Li at 8a slightly deviated from their sites. The redox potential of excess Li insertion (1.5 Li in total) is calculated to be 1.7 V vs. Li^+/Li , which is much lower than at the first stage. Namely, if we consider the average potential in the excess Li insertion, it approximates 2.8 V vs. Li^+/Li ; this suggests that over insertion of Li cations may occur from the beginning of discharge in the actual experiments. Thus, the lower experimental redox potential would be reflected by the mixture of the two insertion stages associated with the kinetics of the Li diffusion. Since Li ions are monovalent, the resultant structures would be determined so as to reduce electrostatic repulsion. As a result, the averaged theoretical lattice constant of $\text{MgLi}_{1.5}\text{Co}_2\text{O}_4$ is 8.56 Å, which is almost the same as that of $\text{Mg}_2\text{Co}_2\text{O}_4$.

Based on the present experimental and theoretical calculation results, we propose the cation-insertion mechanism into the spinel MgCo_2O_4 cathode material in the DSB system, which is comprehensively described for the Mg insertion in our companion paper.¹¹ The insertion reaction of Mg or Li cations is expressed as $\text{MgCo}_2\text{O}_4 + x(\text{M}^{n+} + ne^-) \leftrightarrow (1-x)\text{MgCo}_2\text{O}_4 + x\text{MgMCo}_2\text{O}_4$, where MgCo_2O_4 and MgMCo_2O_4 (M: Mg or Li) exhibit spinel and rocksalt structures, respectively, and the dual-phase equilibrium occurs during discharge/charge process (if M = Mg, MgMCo_2O_4 denotes rocksalt MgCo_2O_4). In this phase separation process, the slight structural change or atomic rearrangement must be also accompanied by the cation insertion. Figure 3(b) illustrates an eccentric insertion process, “intercalation & push-out” process in the DSB system,¹¹ where the Mg/Li cations are intercalated into 16c sites in spinel and the Mg/Co cations in the neighboring 8a

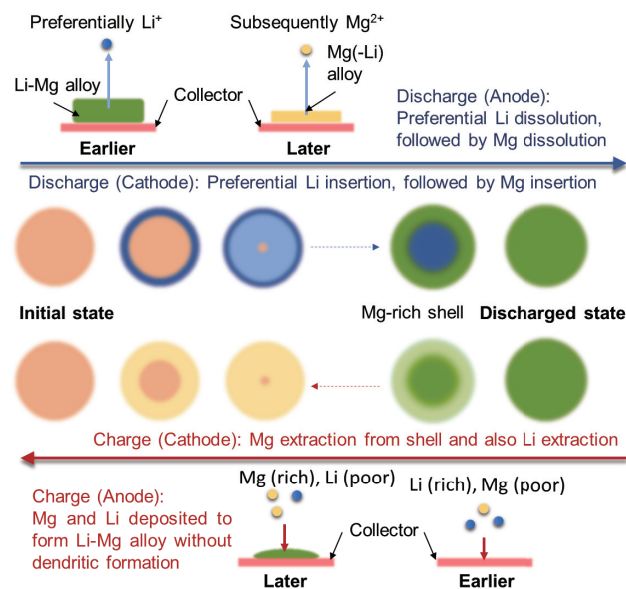


FIG. 4: Discharge and charge processes in the dual-salt battery system. During discharge, Li is preferentially dissolved into the electrolyte, leading to the preferential insertion of Li cations into the cathode. After the condensation of Mg in the alloy, Mg starts to be dissolved, and Mg cations are inserted into the cathode material. On the other hand, during charge, both Li and Mg cations are extracted from the cathode, which leads to the deposition of Li-rich alloy on the anode collector, and subsequently Mg cations are extracted from the cathode and Mg-rich alloy is deposited on the anode-material side. It should be noted that dendritic growth is significantly suppressed even in the deposition of Li-rich alloy.

sites move away to their adjacent 16c sites to circumvent close approach of the cations (by the electrostatic repulsion). Around the Mg/Li-inserted 16c sites, the crystal lattice undergoes the spinel-to-rocksalt transition, thus the atomic-level two-phase equilibrium can be attained, and consequently this structural change would occur coherently, as seen in Fig. 3(c), by which deterioration of the lattice structure would be significantly suppressed.

Our final goal of this project is to produce a rocking-chair-type Mg-Li dual-salt battery, and such a battery system cannot be accomplished unless high potential cathode materials for MRBs such as MgCo_2O_4 are developed. In the present study, we used the beaker cells, in which the amount of the electrolyte is relatively large so that the electrolyte composition is maintained during the redox reactions in both the electrodes. This is, of course, important to show the fundamental electrochemical aspects in the DSB system. However, in the practical battery system, we need to reduce the electrolyte amount as much as possible (ultimately almost zero), which is feasible by using the “rocking-chair type” DSB concept presented here. Figure 4 shows the discharge/charge processes that are reasonably predicted from the present results. In the Li-Mg alloy anode, Li is dissolved preferentially to Mg in terms of the difference in their redox potentials, so that, in the later stage of discharge process, Mg-rich-shell structure would be formed in the cathode material (not only because of the dissolution-potential difference but also because of the slower diffusion of Mg cations in the oxides). During charge, both Mg and Li cations can be extracted from the cathode material from the shell, while Li-Mg alloy (probably Li-rich alloy) are co-deposited with no dendritic formation at the anode side, as shown in Fig. 1. In the combination of MgCo_2O_4 and MgLi alloy, the theoretical electrode energy density would be enlarged up to 600 mWh g^{-1} , which is 4–5 times higher than the

conventional Mg battery and also higher than that of current LIBs. Thus, the rocking-chair type DSB systems would show superior advantages, such as fast diffusion of Li ions and non-dendritic electrodeposition, which would open the way for a metal(alloy)-anode rechargeable battery that combines high energy/power densities.

Methods

Sample preparation

All Spinel oxides were synthesized by the inverse co-precipitation method.^{16,18,19} Aqueous metallic nitrate salt solutions (0.1 L, 0.080 M Mg(II), 0.160 M Co(II)) were prepared by dissolving Mg(NO₃)₂·6H₂O and Co(NO₃)₂·6H₂O in deionized water. A sodium carbonate solution (0.2 L, 0.350 M Na₂CO₃) for pH control and precipitation was also prepared. These solutions were heated to 70–80 °C under vigorous stirring (500 rpm). The metallic nitrate salt solutions were added dropwise into the sodium carbonate precipitation solution. The resulting suspensions were stirred at 70–80°C for 30 min and then filtered. The filtered precipitates (precursors) were rinsed with deionized water (300 cm³) at 80°C to remove completely Na-containing by-products, and air-dried for 24 h at 80°C. The precursors were followed by calcination in air at 350°C for 24h.

Electrochemical tests

Each composite cathode was prepared by coating an Al plate with a mixture of the MgCo₂O₄ (active material), carbon black (as conductive agents), and PVDF (binder) in a weight percent of 80:10:10. Various kinds of beaker cells of three-electrode type were constructed for the electrochemical tests in a glove box whose dew point was below –72°C, where typical weight of the active materials was about 1 mg on 5 mm x 10 mm square and volume of electrolyte was about 2 ml. Mainly we used CsTFSA-based ionic liquids containing Mg(TFSA)₂ and/or LiTFSA salts, where TFSA is bis(trifluoromethanesulfonyl)amide, N(CF₃SO₂)₂⁻. The composition of the electrolyte is denoted as, for example, (Li10/Mg10/Cs80)-TFSA, when the molar percent of the cations in the mixed ionic liquid is Li:Mg:Cs = 10:10:80. The ionic liquid used for the reference electrode was N,N-diethyl-N-methyl-N-(2-methoxyethyl)ammonium bis(trifluoromethanesulfonyl)amide (DEMETFSA). All the electrochemical tests were done with galvanostatic/potentiostatic apparatuses (Biologic, SP-300 and VSP-300) in the glove box.

Structural analysis

The structure of the active material was investigated by X-ray diffraction (XRD; Rigaku, RINT2200) by the irradiation of Cr K α

($\lambda=2.290$ Å). The crystal structure was drawn using VESTA³²⁰, and crystal structure refinement was performed based on the XRD data using the Rietveld program RIETAN-FP²¹.

Ab initio calculations

A series of *ab initio* calculations was performed using the projector augmented-wave (PAW) method²² as implemented in VASP^{23,24}. PAW data sets with radial cutoffs of 1.08, 1.06, 1.22, and 0.80 Å for Li, Mg, Co, and O, respectively, were employed. Li 2s, Mg 3s, Co 3d and 4s, and O 2s and 2p were described as valence electrons. We adopted the Perdew-Burke-Ernzerhof generalized gradient approximation (GGA)²⁵ to density functional theory. For correcting on-site Coulomb interactions in the Co-3d orbitals, we adopted the +*U* scheme proposed by Lichtenstein *et al.*²⁶. Zhou and his colleagues have determined effective *U* values for the Co-3d orbitals to be 5.0–6.3 eV in oxides using a selfconsistent scheme, which can well reproduce the voltage of Li ion batteries within a few tenth eV²⁷. Based on this report, we here selected *U*=6 and *J*=0.88 eV. In all calculations, lattice constants and internal atomic positions were fully optimized until the residual stresses and forces converged to less than 0.3 GPa and 0.02 eV/Å, respectively. Wave functions were expanded with a plane-wave basis set and cutoff energies were set to 550 eV. Spin polarization was considered.

According to the Nernst equation, we calculated the redox potentials of MgCo₂O₄ by Mg insertion as

$$V^{\text{Mg}} = -\frac{1}{2e}[E(\text{Mg}_2\text{Co}_2\text{O}_4) - E(\text{MgCo}_2\text{O}_4) - E(\text{Mg})],$$

and by Li insertion as

$$V^{\text{Li}} = -\frac{1}{e}[E(\text{LiMgCo}_2\text{O}_4) - E(\text{MgCo}_2\text{O}_4) - E(\text{Li})],$$

where *e* (> 0) is the elementary charge, and *E* is the total energy. In addition, we modeled Li_{1.5}MgCo₂O₄ containing excess Li ions and calculated its redox potential as

$$V_{\text{ex}}^{\text{Li}} = -\frac{1}{0.5e}[E(\text{Li}_{1.5}\text{MgCo}_2\text{O}_4) - E(\text{LiMgCo}_2\text{O}_4) - 0.5E(\text{Li})].$$

Acknowledgements

The authors would like to thank Ms. Chiharu Hirao for her experimental help. This work was supported by the Advanced Low Carbon Technology Research and Development Program (ALCA), JSPS Grant-in-Aid for Scientific Research (B) No. 26289280, Grant-in-Aid from the Special Coordination Funds for Promoting Science and Technology commissioned by JST, MEXT of Japan, and the MEXT Elements Strategy Initiative to Form Core Research Center. Computing resources of ACCMS at Kyoto University were used in this work.

¹ D. Aurbach, Z. Lu, A. Schechter, Y. Gofer, H. Gizbar, R. Turgeman, Y. Cohen, M. Moshkovich and E. Levi, *Nature*, 2000, **407**, 724–727.
² J.-M. Tarascon and M. Armand, *Nature*, 2011, **414**, 359–367.
³ M. Matsui, *J. Power Sources*, 2011, **196**, 7048–7055.
⁴ S. Yagi, A. Tanaka, T. Ichitsubo and E. Matsubara, *ECS Electrochem Lett.*, 2014, **1**(2), D11–D14.
⁵ M. Morita, N. Yoshimoto, S. Yakushiji and M. Ishikawa, *Electrochem. Solid-State Lett.*, 2001, **4**(11), A177–A179.

⁶ S. Yagi, T. Ichitsubo, Y. Shirai, S. Yanai, T. Doi, K. Murase and E. Matsubara, *J. Mater. Chem. A*, 2014, **2**, 1144–1149.
⁷ Y. Cheng, Y. Shao, J.-G. Zhang, V.L. Sprenkle, J. Liu and G. Li, *Chem. Commun.*, 2014, **50**, 9644–9646.
⁸ T. Gao, F. Han, Y. Zhu, L. Suo, C. Luo, K. Xu and C. Wang, *Adv. Energy Mater.*, 2014, **4**, 1401507.
⁹ J.-H. Cho, M. Aykol, S. Kim, J.-H. Ha, C. Wolverton, K.Y. Chung, K.-B. Kim and B.-W. Cho, *J. Am. Chem. Soc.*, 2014, **136**, 16116–16119.

- ¹⁰ B. Gao, T. Nohira, R. Hagiwara and Z. Wang, Molten Salts Chemistry and Technology, M. Gaune-Escard and G. M. Haarberg eds., *John Wiley & Sons, Ltd.*, 2014, Chapt. 5.4.
- ¹¹ S. Okamoto, T. Ichitsubo, T. Kawaguchi, Y. Kumagai, K. Shimokawa, F. Oba, S. Yagi, K. Shimokawa, N. Goto, T. Doi, E. Matsubara, *To be submitted*
- ¹² D. Aurbach, M.D. Levi and E. Levi, *Sol. Stat. Ionics*, 2008, **179**, 742–751.
- ¹³ T. Ichitsubo, S. Yagi, R. Nakamura, Y. Ichikawa, S. Okamoto, K. Sugimura, T. Kawaguchi, A. Kitada, M. Oishi, T. Doi and E. Matsubara, *J. Mater. Chem.*, 2014, **2**, 14858–14866.
- ¹⁴ P. Novák and J. Desilvestro, *J. Electrochem. Soc.*, 1993, **140**(1), 140–144.
- ¹⁵ T.D. Gregory, R.J. Hoffman and R. Winterton, *J. Electrochem. Soc.*, 1990, **137**(3), 775–780.
- ¹⁶ T. Ichitsubo, T. Adachi, S. Yagi and T. Doi, *J. Mater. Chem.*, 2011, **21**, 11764–11772.
- ¹⁷ M. Oishi, S. Okamoto, T. Ichitsubo, S. Toyoda, E. Matsubara, T. Nohira and R. Hagiwara, *J. Electrochem Soc.*, 2014, **161**, A943–947.
- ¹⁸ S. Yagi, Y. Ichikawa, I. Yamada, T. Doi, T. Ichitsubo and E. Matsubara, *Jpn. J. Appl. Phys.*, 2013, **52**, 025501.
- ¹⁹ N. Kamioka, T. Ichitsubo, T. Uda, S. Imashuku, Y. Taninouchi and E. Matsubara, *Mater. Trans.*, 2008, **49**, 824–828.
- ²⁰ K. Momma and F. Izumi, *J. Appl. Crystallogr.*, 2011, **44**, 1272–1276.
- ²¹ F. Izumi and K. Momma, *Solid State Phenom.*, 2007, **130**, 15–20.
- ²² P.E. Blöchl, *Phys. Rev. B*, 1994, **50**, 17953–17979.
- ²³ G. Kresse and J. Furthmüller, *Phys. Rev. B*, 1996, **54**, 11169–11189.
- ²⁴ G. Kresse and D. Joubert, *Phys. Rev. B*, 1999, **59**, 1758–1775.
- ²⁵ J.P. Perdew, K. Burke and M. Ernzerhof, *Phys. Rev. Lett.*, 1996, **77**, 3865–3868.
- ²⁶ A.I. Liechtenstein, V. I. Anisimov and J. Zaanen, *Phys. Rev. B*, 1995, **52**, R5467–R5470.
- ²⁷ F. Zhou, M. Cococcioni, C.A. Marianetti, D. Morgan and G. Ceder, *Phys. Rev. B*, 2004, **70**, 235121.